Thin Insulating Tunneling Contacts for Efficient and Water-Resistant Perovskite Solar Cells

*Qi Wang, Qingfeng Dong, Tao Li, Alexei Gruverman, and Jinsong Huang**

Organolead trihalide perovskite (OTP) materials have drawn tremendous attention in the past years because of their great promise to fabricate next generation of low-cost and highly efficient solar cells.[1,2] The power conversion efficiency (PCE) of perovskite solar cells has rocketed in the last few years, which has been ascribed to the excellent optoelectronic properties and unique defects physics that originates the low carrier recombination in perovskite polycrystalline thin films.[3] Charge recombination in the grain interior can be negligible due to the absence of deep traps in OTP grains which also enables a carrier diffusion length significantly longer than the optical attenuation length in their single crystals.[2,4] Even in polycrystalline perovskite thin films, the carrier diffusion lengths can still be much longer than the light penetration length, thanks to the enlarging grains and improving crystallinity of the perovskite films with recent rapid improvement in material morphology controlling.[5,6] The enlargement of grains also significantly reduces carrier recombination at perovskite grain boundaries (GBs), which is facilitated by the advance of passivation techniques to further reduce recombination at GBs and film surface.[7] Now that the photogenerated carriers can flow through perovskite films with negligible charge recombination, minimizing the charge recombination at the contacts becomes increasingly important to achieve highly efficient perovskite solar cells.

Inspired by the success of applying tunneling contacts in silicon solar cells, in this paper, we report an insulating tunneling layer inserted between the perovskite and the electron collection layer in perovskite solar cells can reduce charge recombination. Many insulating polymers, including commercial plastic foam which is broadly used for packaging, can form a tunneling contact at the cathode side. The tunneling contact allows the transport of electrons from perovskite to cathode, while block holes into the perovskite layer. Devices with these insulating materials exhibited an increased PCE of 20.3% under 1 sun illumination. This simple nonlattice-matching structure enables the capping of the perovskite films by superhydrophobic insulating layers, which dramatically enhances resistance of perovskite solar cells to water-caused damage without further encapsulation.

The tunneling junctions applied in silicon solar cells, which resulted in the most efficient silicon solar panels in the world, are comprised of an insulating oxide or a thin-layer of amorphous silicon (HIT structure) inserted between the intrinsic silicon and the heavily-doped silicon layer or indium-tin-oxide (ITO) layer. The tunneling junctions have been shown to suppress the charge recombination at contacts and passivate the surface to increase device efficiency.[8] The inserted insulating layer can selectively conduct one type of charges while block the other type, which spatially separates photogenerated electrons and holes to reduce their recombination, because the charge selection electrodes or charge transport layers have energy-matching electronic states for one type of charges to tunnel into but not for the other type.[9] The oxide or amorphous silicon layers are generally deposited by relatively high temperature vacuum process, which is however not compatible for perovskite solar cells. Encouragingly, we found that the low temperature solution-coated polymeric insulating layers could play the same function, which potentially makes it low-cost and simple to be applied. **Figure 1**a shows the structure of the devices in this study where the tunneling junction locates at the cathode side. An insulating polymer is inserted between the perovskite and the electron collecting fullerene (C_{60}) layers, and the proposed energy diagram in Figure 1b is also shown to illustrate the function of insulating layer in transporting electrons and blocking holes in the perovskite layer. Photogenerated electrons at conduction band minimal (CBM) of the perovskite layer can tunnel to the excited electronic states in C_{60}, followed by their relaxation to the lowest unoccupied molecular orbital (LUMO) of C_{60}, because there are energy-matching unoccupied states in C_{60} for electrons to tunneling into. On the contrary, these are no energy-matching states in C_{60} which could allow the holes to tunnel into. Therefore, the tunneling rate of holes from perovskite to C_{60} will be very low. The thin insulating layer thus allows the transport of photogenerated electrons in perovskite to C_{60} layer by tunneling, and also blocks the photogenerated holes back into the perovskite layer. Therefore, the insulating tunneling layer causes a spatial separation of the photogenerated electrons and holes, which reduces their recombination at the contact of the perovskite and electron transport layers.

The perovskite films in this study were made by the interdiffusion method.[10] Poly(triaryl amine) (PTAA) was chosen as the hole transporting layer because of the much larger perovskite grain size formed on the non-wetting surface of PTAA.[5] The PTAA film was doped by 1.0 wt% 2,3,5,6-Tetrafluoro-7,7,8,8-tetracyanoquinodimethane (F4-TCNQ) to increase its conductivity,

Q. Wang, Dr. Q. Dong, Prof. J. Huang
Department of Mechanical and Materials Engineering
University of Nebraska-Lincoln
Lincoln, NE 68588, USA
E-mail: jhuang2@unl.edu
Dr. T. Li, Prof. A. Gruverman
Department of Physics and Astronomy
University of Nebraska-Lincoln
Lincoln, NE 68588, USA

DOI: 10.1002/adma.201600969

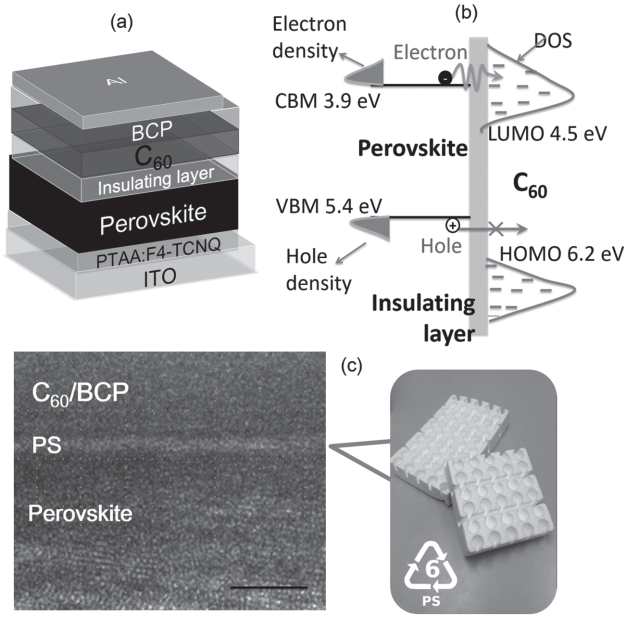

Figure 1. a) The device structure of perovskite solar cells and b) the energy diagram that illustrates the principle of suppressing surface charge recombination by the insulating layer. The insulating layer suppresses charge recombination by separating the excess electrons and holes in the electron transport layer and perovskite layer, respectively; c) A transmission electron microscopy cross-section image of a 19.6% efficiency device revealing the presence of 1–2 nm PS layer between perovskite and electron transport layer. The scale bar is 5 nm. The PS layer was made from commercial PS plastic foam, the picture of which was also shown on the right.

which was found important in increasing perovskite device fill factor.[11] Three insulating polymers, polystyrene (PS), Teflon, and polyvinylidene-trifluoroethylene copolymer (PVDF-TrFE), were randomly chosen for the tunneling materials in this study. The molecular structures are shown in Figure S1 of the Supporting Information. The details of device fabrication can be found in the Experimental Section. The insulating polymers spun on the perovskite films could form a conformal tunneling layer, as verified by the high resolution transmission electron microscopy (TEM) cross-section image of the devices. As shown in Figure 1c, the spun PS layer with a thickness of 1–2 nm conformably covers the perovskite layer. The scanning electron microscopy (SEM) images of a perovskite film before and after depositing PS insulating layer were shown in Figure S2 of the Supporting Information, which reveals a good coverage of the perovskite film by PS at micrometer scale.

Figure 2a shows the photocurrent curves of perovskite devices with different insulating polymers inserted and that of the control device with 20 nm [6]-phenyl-C61-butyric acid methyl ester (PCBM) to replace the insulating polymer layer. The control device has a short-circuit current density (J_{SC}) of 21.1 mA cm^{-2}, an open-circuit voltage (V_{OC}) of 1.07 V, a fill factor (FF) of 74.9%, and a PCE of 16.9%, which represent a typical performance of PCBM passivated perovskite devices.[11] In a striking contrast, the devices with polymer tunneling contacts exhibited an increased J_{SC} and FF. The devices with PS, PVDF-TrFE, and Teflon tunneling layer showed higher J_{SC} of 22.9, 22.9, and 22.8 mA cm^{-2}, respectively. Meanwhile, the FFs for devices with inserted PS, PVDF-TrFE, and Teflon tunneling contacts were also increased to 79.6%, 77.6%, and 75.6%, respectively. The performances of perovskite devices with different tunneling layers were also summarized in **Table 1**. It should be mentioned that the V_{OC} of the perovskite devices with tunneling contacts fabricated from different batches slightly varied between 1.05 and 1.11 V. Statistic V_{OC} distributions of 50 samples in Figure S3 of the Supporting Information show that the devices with tunneling contacts have a higher average V_{OC} of 1.07 V, compared with 1.05 V of the control devices. The statistics of PCE in Figure 2b, J_{SC}, FF distributions in Figure S3 of the Supporting Information demonstrate the reliability and the repeatability of the performance enhancement by the tunneling contacts. The universal performance enhancement by different insulating polymers and no change of trap density measured by thermal admittance spectroscopy belittle the possibility of chemical bonding formation between perovskite and the insulating polymers, because chemical reaction should be sensitive to the chemical structure of the polymers. It indicates the polymer only physically contact to the perovskite and act as tunneling layer. It was interesting that the PS plastic foam, which is broadly used for packaging, worked as well to get a PCE more than 19.0%. A picture of the PS plastic foam used in this study is shown in Figure 1c. The perovskite device with PS from dissolved foam as the tunneling layer exhibited a J_{SC} of 22.9 mA cm^{-2}, a V_{OC} of 1.07 V, a FF of 80.3%, and a PCE of 19.6%. The device performance is even slightly higher than those of the devices with other three polymers with higher purity. The release of constraint of high material purity for highly efficient perovskite devices might make perovskite solar cells even more competitive in the future market.

Since the tunneling probability strongly depends on tunneling-layer thickness, the thickness of the tunneling layer should significantly influence the electron extraction efficiency and thus device efficiency.[12] Figure 2c shows the photocurrent curves of perovskite devices with PS layers of different thicknesses which were tuned by varying the concentration of PS solution in the spin-coating process. As shown in Figure 2c, for PS solution with a concentration of 0.02%, the device showed a J_{SC} of 20.8 mA cm^{-2}, a V_{OC} of 1.05 V, a FF of 75.1% and a PCE of 16.4%, which is comparable to that of the PCBM-passivated devices. This can be explained by the fact that the PS layer formed from the solution with such low PS concentration is barely continuous, and thus the device resembles the control device without PS layer. When the PS concentration was increased to 0.1%, 0.5%, and 1.0%, the photocurrents were significantly increased to 22.0, 22.8, and 22.9 mA cm^{-2}, respectively. The best devices were made by 1.0% PS solution, exhibiting a V_{OC} of 1.10 V, a J_{SC} of 22.9 mA cm^{-2}, a FF of 80.6%, and a PCE of 20.3% from the photocurrent scanning. For these devices, the PS layer thickness was estimated to be 1–2 nm from the high resolution TEM shown in Figure 1c. Further increasing PS layer thickness severely reduced the J_{SC}, V_{OC}, and FF to 20.0 mA cm^{-2}, 1.03 V, and 49.0%, respectively, because the increased tunneling layer thickness reduced electron tunneling rate. Figure 2d show the average external quantum efficiency (EQE) spectrum of devices with PS and PCBM as the contact layer. Figure 2e shows the steady photocurrent and

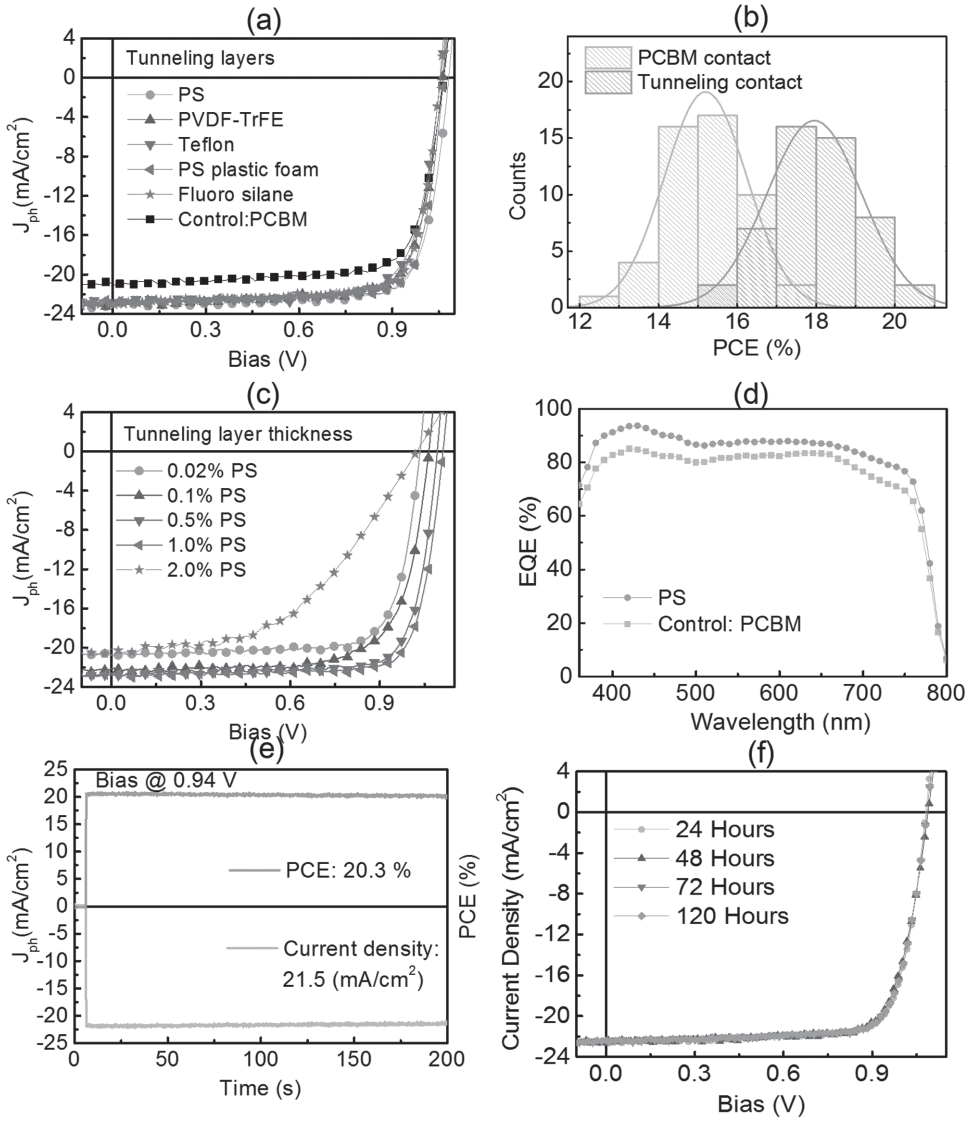

Figure 2. a) Current density–voltage (*J–V*) characteristics of the devices with different insulating tunneling contacts. The control device has 20 nm PCBM to replace the insulating layer; b) The statistics of PCE distribution for perovskite devices with PCBM (50 samples) and tunneling contact (50 samples). c) *J–V* of the devices with PS layers of different thicknesses. The voltage scanning direction in the *J–V* measurement was from negative bias to positive bias; d) Average EQE of 10 devices with a tunneling layer, and average EQE of 10 control devices with a PCBM contact layer. The EQE curves of the devices could be found in the Supporting Information; e) Steady-state measurement of J_{SC} and PCE for the best device with a PS tunneling layer. f) Stability test of a perovskite device with PS tunneling layer. The legend in the figure represents the air exposure time after the device was tested after being fabricated. The average humidity of atmosphere was ≈40%.

PCE measured at the maximum power output point (0.94 V) of the most efficient device. The steady photocurrent, stabilized PCE measured at the maximum power point agrees well with that measured from *J–V* scanning, excluding the existence of photocurrent hysteresis in our devices and confirming the accuracy of our device efficiency characterization. The absence of photocurrent hysteresis of these devices is also confirmed by changing the photocurrent scanning directions (Figure S5, Supporting Information). We recently demonstrated that ion migration at grain boundaries plays a dominant role in causing the photocurrent hysteresis.[13] Any material which can block the ion migration channel at grain boundaries is expected to eliminate the photocurrent hysteresis.

The insulating polymer may serve as a water-resistant layer to protect the perovskite film from water damage. The speculation stemmed from the observation that the perovskite devices with insulating polymers generally showed a better stability in air (Figure 2f), while the control devices without insulating polymers always degraded to yellow color in several days.[14] To confirm it, we chose a hydrophobic insulating fluoro-silane, Trichloro(3,3,3-trifluoropropyl)silane, as a tunneling layer to make water-resistant devices. The fluoro groups make the material to be extremely hydrophobic.[15] In addition, it has been reported fluoro-silane could undergoes a cross-linking process with the aid of tiny amount of moisture.[15,16] **Figure 3**a illustrates the cross-linking process of this material.

Table 1. Performance of devices with different insulating tunneling layers.

Tunneling contacts	J_{SC} [mA cm^{-2}]	V_{OC} [V]	FF [%]	PCE [%]
0.02% PS	20.8	1.05	75.1	16.4
0.1% PS	22.0	1.07	73.0	17.2
0.5% PS	22.8	1.09	76.5	19.2
1.0% PS	22.9	1.10	80.6	20.3
2.0% PS	20.0	1.03	49.0	10.1
PVDF-TrFe	22.9	1.06	77.6	18.8
Teflon	22.8	1.05	75.6	18.1
PS plastic foam	22.9	1.07	80.3	19.6
Fluoro-silane	22.7	1.05	79.3	18.9
Control (PCBM)	21.1	1.07	74.9	16.9

When fluoro-silane was deposited on top of the perovskite films, tiny amount of H_2O that exists in the perovskite films will trigger the hydroxylation of silanes to form silanols. Then the silanols will automatically undergoes a cross-linking process by forming Si–O–Si (siloxane) bonds, which makes this insulating layer robust to protect the underneath perovskite films from water attacking. The devices with the fluoro-silane layer also showed a good efficiency of 18.9% (Figure 2a), which is comparable to the performance of devices with other types of tunneling contacts. Encouragingly, the hydrophobic polymer protected devices showed much better resistance to water damage. As shown by the photos in Figure 3b,c, the perovskite device with fluoro-silane layer without further encapsulation showed negligible color change after it was soaked in water for 3 min, while the control device with 20 nm PCBM changed to yellow color after it was immersed in water for less than 5 s. The operation of the unencapsulated device in water was also demonstrated in Figure 3d, showing a V_{OC} of 1.09 V which is slightly higher than that of the device measured under one sun condition (Figure 2a). The slight variation in V_{OC} might be caused by the optical effect of the water or glass beaker which slightly change the light illumination intensity to increase device V_{OC}. The stable operation of the perovskite devices in water indicates the very good conformal coating of the nanometer thick insulting layer onto perovskite layers. Improving the moisture stability of perovskite solar cells has drawn great research attention recently.[17] The demonstration of stable device operation in water represents a major progress in stabilizing the perovskite solar cells in addition to the improved stability in air or moisture, though atomic conformal coverage of the perovskite by the polymer without any pin-holes is still challenging to achieve over very large device area with spin-coating.

The performance enhancement in our devices is primarily ascribed to the function of tunneling layer in extracting electrons and blocking holes. To demonstrate that, conductive atomic force microscopy (c-AFM) measurement was conducted to characterize the local dark-current and photocurrent of perovskite samples with or without PS tunneling layer at nanoscopic level. The samples for dark-current measurements have the structure of ITO/PTAA: F4-TCNQ/perovskite/with or without PS. Since both PTAA and the Pt-coated AFM conductive tip have a high work function as well, the measured current is essentially a hole current. As shown in **Figure 4**a,b, the local dark current reduced after coating the PS layer, proving the function of PS in blocking holes. The uniform reduction of hole current across the whole mapping area indicates a conformal coating of PS on the perovskite film. The samples for photocurrent measurement had the structure of ITO/PTAA:F4-TCNQ/perovskite/with or without PS/C_{60}. In the

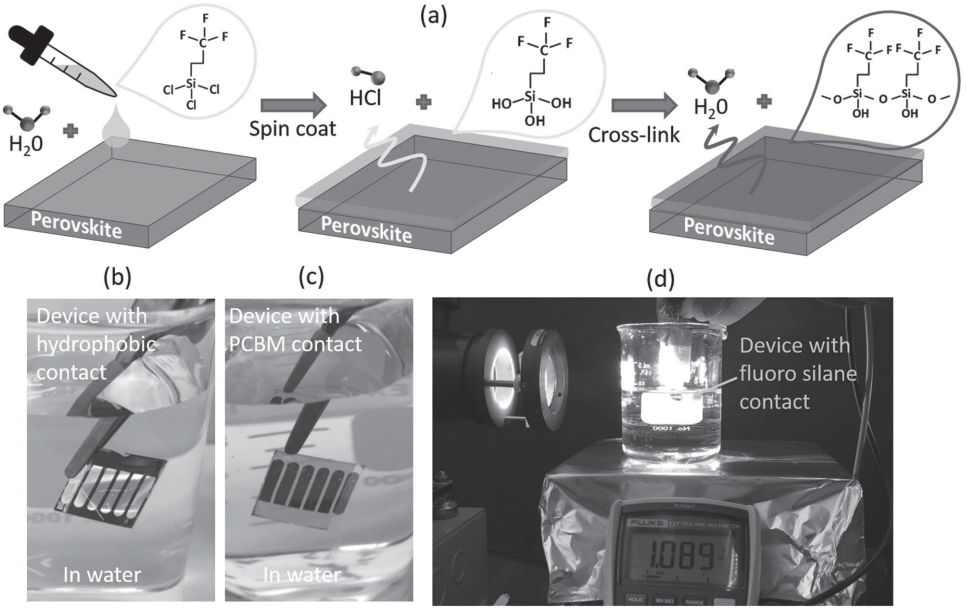

Figure 3. a) Schematic diagram showing the cross-link process of fluoro-silane layer on the perovskite film. b) A picture of the perovskite device with fluoro-silane layer. The picture was taken after dipping the device in water for 1–2 min. c) A picture of the perovskite device without tunneling layer. The picture was taken after dipping the device in water for 5 s. d) A picture showing the perovskite device with fluoro-silane layer had a 1.09 V photovoltage output in water.

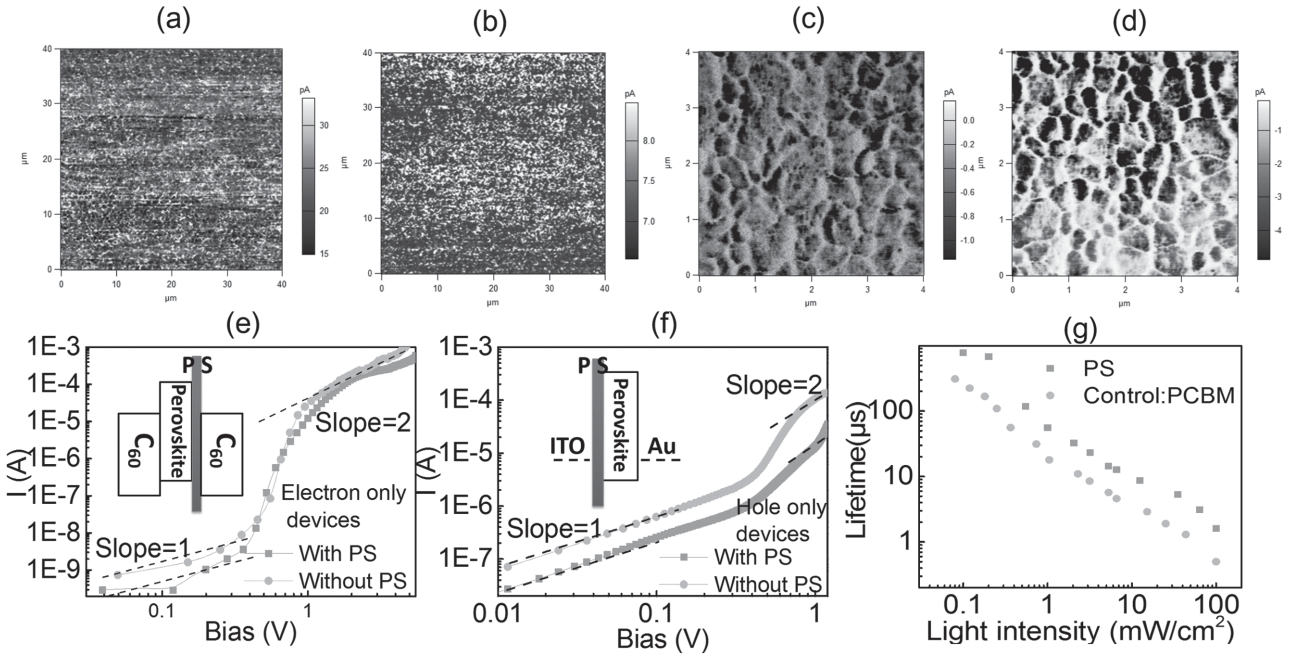

Figure 4. c-AFM measurement of the local dark-current of the samples with the structures of a) ITO/PTAA:F4-TCNQ/perovskite, b) ITO/PTAA:F4-TCNQ/perovskite/PS. c) c-AFM measurement of the local photocurrent of samples with the structure of ITO/PTAA:F4-TCNQ/perovskite/C_{60}, and d) ITO/PTAA:F4-TCNQ/perovskite/PS/C_{60}. Note that the photocurrent in (c) and (d) has a minus value because circuit connection followed that of the *J–V* curve measurement in Figure 2a,b; Current–voltage (*I–V*) characteristics of e) electron-only device and f) hole-only device. The insets of (e) and (f) show the structures of electron-only and hole-only devices, respectively. g) Carrier recombination lifetime of perovskite devices with or without PS tunneling layer measured by TPV.

measurement, the c-AFM tips contacted C_{60} surface to map the photocurrent of samples illuminated by a white light source with an intensity of 20 mW cm^{-2}. Since there is an electron-accepting layer, electrons can be collected by C_{60} and conduct to the tip. Figure 4c,d shows the photocurrent mapping results of the perovskite samples without or with the PS tunneling layer, respectively. The samples without PS tunneling layer showed a photocurrent ranging from 0 to 0.8 pA with a very good reproducibility. After inserting a PS contact, the local photocurrent through most grains increased to >4 pA, directly proving the function of PS tunneling layer in enhancing the photocurrent output. The function of the tunneling layer is also confirmed at macroscopic level using the single-carrier devices with or without PS tunneling layer. The electron only devices have the structure of ITO/C_{60}/perovskite/with or without PS/C_{60}/Al, and the hole only devices have the structure of ITO/with or without PS/perovskite/Au, which are shown in the insets of Figure 4e,f.

The tunneling layer spatially separates photogenerated electrons and holes at the perovskite/polymer interface by transporting electrons and blocking holes, which should lead to the reduction of the carrier surface recombination. To verify it, we compared the carrier recombination lifetimes of devices with or without PS contact by transient photovoltage spectroscopy (TPV). As shown in the Figure 4g, carrier recombination lifetime is longer in the device with PS tunneling contact, compared with the control device (PCBM passivated) at all the light intensity range. The carrier lifetime of the control device under one sun illumination is 0.5 μs which corresponds to the typical TPV lifetime of the PCBM passivated devices.[18] The device with PS contact have a much longer carrier lifetime of 1.6 μs under one sun illumination, demonstrating the suppressed carrier recombination in devices with the tunneling contacts. The increased carrier lifetime extends the carrier diffusion length to increase device J_{SC} and FF. Meanwhile, the suppressed carrier recombination is also beneficial to the increase of V_{OC} as observed in the devices with tunneling contacts.

In conclusion, we demonstrated that inserting a tunneling layer between perovskite and electron transport layer could significantly increase device performance by suppressing carrier recombination at the cathode contact. The tunneling layer can also serve as an encapsulation layer to prevent perovskite film from damage caused by water or moisture. This method is simple because it does not need lattice matching between the buffer layer and perovskite. The low temperature solution process makes it compatible with many types of perovskite materials, and may be applied for anode contact as well. The freedom to choose any insulating layer for contact enables more device designs and manufacturing.

Supporting Information

Supporting Information is available from the Wiley Online Library or from the author.

Acknowledgements

Q.W. and Q.D. contributed equally to this work. The authors thank the financial support from National Science Foundation (DMR-1505535 and

DMR-1420645), Department of Energy (DE-EE0006709), and Office of Naval Research (N00014-15-1-2713).

Received: February 18, 2016
Revised: March 16, 2016
Published online: May 17, 2016

[1] a) M. A. Green, A. Ho-Baillie, H. J. Snaith, *Nat. Photonics*, **2014**, *8*, 506; b) J. H. Heo, S. H. Im, J. H. Noh, T. N. Mandal, C.-S. Lim, J. A. Chang, Y. H. Lee, H.-J. Kim, A. Sarkar, M. K. Nazeeruddin, *Nat. Photonic s* **2013**, *7*, 486; c) M. M. Lee, J. Teuscher, T. Miyasaka, T. N. Murakami, H. J. Snaith, *Science* **2012**, *338*, 643.

[2] H. J. Snaith, *J. Phys. Chem. Lett.* **2013**, *4*, 3623.

[3] a) W. J. Yin, T. Shi, Y. Yan, *Adv. Mater.* **2014**, *26*, 4653; b) C. Wehrenfennig, G. E. Eperon, M. B. Johnston, H. J. Snaith, L. M. Herz, *Adv. Mater.* **2014**, *26*, 1584; c) C. S. Ponseca Jr., T. J. Savenije, M. Abdellah, K. Zheng, A. Yartsev, T. r. Pascher, T. Harlang, P. Chabera, T. Pullerits, A. Stepanov, *J. Am. Chem. Soc.* **2014**, *136*, 5189; d) D. Bi, W. Tress, M. I. Dar, P. Gao, J. Luo, C. Renevier, K. Schenk, A. Abate, F. Giordano, J.-P. C. Baena, *Sci. Adv.* **2016**, *2*, e1501170.

[4] a) Q. Dong, Y. Fang, Y. Shao, P. Mulligan, J. Qiu, L. Cao, J. Huang, *Science* **2015**, *347*, 967; b) D. Shi, V. Adinolfi, R. Comin, M. Yuan, E. Alarousu, A. Buin, Y. Chen, S. Hoogland, A. Rothenberger, K. Katsiev, *Science* **2015**, *347*, 519; c) S. De Wolf, J. Holovsky, S.-J. Moon, P. Löper, B. Niesen, M. Ledinsky, F.-J. Haug, J.-H. Yum, C. Ballif, *J. Phys. Chem. Lett.* **2014**, *5*, 1035.

[5] C. Bi, Q. Wang, Y. Shao, Y. Yuan, Z. Xiao, J. Huang, *Nat. Commun.* **2015**, *6*, 7747.

[6] a) H. Yu, F. Wang, F. Xie, W. Li, J. Chen, N. Zhao, *Adv. Funct. Mater.* **2014**, *24*, 7102; b) H. Zhou, Q. Chen, G. Li, S. Luo, T.-B. Song, H.-S. Duan, Z. Hong, J. You, Y. Liu, Y. Yang, *Science* **2014**, *345*, 542; c) B. Yang, O. Dyck, J. Poplawsky, J. Keum, A. Puretzky, S. Das, I. Ivanov, C. Rouleau, G. Duscher, D. Geohegan, *J. Am. Chem. Soc.* **2015**, *137*, 9210; d) W. S. Yang, J. H. Noh, N. J. Jeon, Y. C. Kim, S. Ryu, J. Seo, S. I. Seok, *Science* **2015**, *348*, 1234; e) F. Wang, H. Yu, H. Xu, N. Zhao, *Adv. Funct. Mater.* **2015**, *25*, 1120; f) Z. Xiao, Q. Dong, C. Bi, Y. Shao, Y. Yuan, J. Huang, *Adv. Mater.* **2014**, *26*, 6503.

[7] a) Y. Shao, Z. Xiao, C. Bi, Y. Yuan, J. Huang, *Nat. Commun.* **2014**, *5*, 5784; b) J. Xu, A. Buin, A. H. Ip, W. Li, O. Voznyy, R. Comin, M. Yuan, S. Jeon, Z. Ning, J. J. McDowell, *Nat. Commun.* **2015**, *6*, 7081; c) N. K. Noel, A. Abate, S. D. Stranks, E. S. Parrott, V. M. Burlakov, A. Goriely, H. J. Snaith, *ACS Nano* **2014**, *8*, 9815.

[8] a) K. Masuko, M. Shigematsu, T. Hashiguchi, D. Fujishima, M. Kai, N. Yoshimura, T. Yamaguchi, Y. Ichihashi, T. Mishima, N. Matsubara, *IEEE J. Photovoltaics* **2014**, *4*, 1433; b) D. L. Pulfrey, *IEEE Trans. Electron Dev.* **1978**, *25*, 1308.

[9] a) T. Schulze, L. Korte, E. Conrad, M. Schmidt, B. Rech, *J. Appl. Phys.* **2010**, *107*, 023711; b) A. K. Chandiran, N. Tetreault, R. Humphry-Baker, F. Kessler, E. Baranoff, C. Yi, M. K. Nazeeruddin, M. Grätzel, *Nano Lett.* **2012**, *12*, 3941.

[10] Z. Xiao, C. Bi, Y. Shao, Q. Dong, Q. Wang, Y. Yuan, C. Wang, Y. Gao, J. Huang, *Energy Environ. Sci.* **2014**, *7*, 2619.

[11] Q. Wang, C. Bi, J. Huang, *Nano Energy* **2015**, *15*, 275.

[12] a) I. D. Parker, *J. Appl. Phys.* **1994**, *75*, 1656; b) Z. Xu, X. Bai, E. Wang, Z. L. Wang, *Appl. Phys. Lett.* **2005**, *87*, 163106.

[13] Y. Shao, Y. Fang, T. Li, Q. Wang, Q. Dong, Y. Deng, Y. Yuan, H. Wei, M. Wang, A. Gruverman, J. Shield, J. Huang, *Energy Environ. Sci.* **2016**, 10.1039/C6EE00413J.

[14] R. Dong, Y. Fang, J. Chae, J. Dai, Z. Xiao, Q. Dong, Y. Yuan, A. Centrone, X. C. Zeng, J. Huang, *Adv. Mater.* **2015**, *27*, 1912.

[15] a) M. Pagliaro, R. Ciriminna, *J. Mater. Chem.* **2005**, *15*, 4981; b) H. Maciejewski, J. Karasiewicz, M. Dutkiewicz, M. Nowicki, *RSC Adv.* **2014**, *4*, 52668.

[16] J. van Wijk, N. van Deventer, E. Harmzen, J. Meuldijk, B. Klumperman, *J. Mater. Chem. B* **2014**, *2*, 4826.

[17] a) S. Yang, Y. Wang, P. Liu, Y.-B. Cheng, H. J. Zhao, H. G. Yang, *Nat. Energy* **2016**, *1*, 15016; b) J. You, L. Meng, T.-B. Song, T.-F. Guo, Y. M. Yang, W.-H. Chang, Z. Hong, H. Chen, H. Zhou, Q. Chen, *Nat. Nanotechnol.* **2016**, *11*, 75; c) W. Chen, Y. Wu, Y. Yue, J. Liu, W. Zhang, X. Yang, H. Chen, E. Bi, I. Ashraful, M. Grätzel, *Science* **2015**, *350*, 944.

[18] Y. Shao, Y. Yuan, J. Huang, *Nat. Energy* **2016**, *1*, 15001.